Improving frequency stability using slowly modulated adaptive feedback

Harry Dankowicz*

Department of Mechanical Science and Engineering,
University of Illinois at Urbana-Champaign, Urbana, IL 61801 and
Department of Mechanical Engineering,
University of Maryland, College Park, MD 20742

Steven W. Shaw

Department of Mechanical and Civil Engineering,
Florida Institute of Technology, Melbourne, FL 32901
Department of Mechanical Engineering,
Michigan State University, East Lansing, MI 48824 and
Department of Physics and Astronomy,
Michigan State University, East Lansing, MI 48824

Oriel Shoshani

Department of Mechanical Engineering,
Ben-Gurion University of the Negev, Beer-Sheva 84105, Israel

Author-accepted manuscript (AAM) of
Dankowicz, H., Shaw, S.W., and Shoshani, O. (2026) "Improving frequency stability using slowly modulated adaptive feedback,"
Physical Review Applied 25(5), 054050.

Abstract

We present a new method for improving frequency stability in a self-sustained oscillator using a secondary feedback loop acting outside the main sustaining loop with adaptively-controlled amplitude and phase shift. We show that quite simple adaptive control laws for the control states of the secondary feedback signal can affect the way that noise circulates in the oscillator so as to reduce or even eliminate (in theory) phase diffusion, i.e., the rate of linear growth with time of the variance of the oscillator output phase. Our rigorous treatment of this effect is based on a linearized analysis of the noisy slow-flow amplitude and phase equations for a relevant general class of systems, from which we derive an explicit expression for the corresponding asymptotic rate of phase diffusion. Using this result, we consider different choices for tailoring the actuation from the secondary feedback loop. This includes tuning a phase coupling constant that ensures that the noise driving the output phase also drives one of the adaptive control states, which represents a generalization of a desirable behavior observed in internally resonant coupled mode operation. We show that such feedback design may be used to eliminate effects that commonly arise from the conversion of amplitude fluctuations to phase diffusion, analogous to operation at zero dispersion points, and to improve upon the phase cleaning effect associated with internal resonance to even achieve the ideal situation of zero phase diffusion. We validate our theoretical findings with numerical simulations that agree remarkably well with the theory. The presented results establish a framework for achieving extraordinary frequency stability using slowly varying states of the resonator and feedback.

I. INTRODUCTION

Oscillator frequency stability is an essential feature for many modern technologies, including navigation, computing, network operations, telecommunications, and scientific measurements [1]. Frequency synthesis is achieved using a self-sustained oscillator of a desired period. The oscillator is built from a resonant device that sets the frequency and a means of countering dissipation to maintain the oscillation, typically by a feedback loop that contains an energy source. Important qualities of these systems include size, power usage, cost,

* Contact author: danko@umd.edu

robustness to environmental conditions, and precision (frequency stability). Short-term frequency stability is determined by the effects of noise in the resonator and the sustaining elements [2].

An ideal oscillator would output a perfectly periodic signal; however, the presence of noise results in fluctuations in the periodicity of the output signal. These fluctuations are commonly quantified by different measures including the frequency spectrum of the output, which has a finite linewidth rather than the ideal delta function at the desired frequency; computing the Allan variance, which calculates precision over different timescales; or looking at the rate of phase diffusion, which is a consequence of the lack of dynamic rigidity of the dynamics tangent to the limit cycle that describes the self-oscillation. All of these measures are interrelated [3].

The resonator element of an oscillator is characterized by the properties of the vibration mode of interest, specifically its natural frequency, dissipation rate (or Q value), and Duffing nonlinearity. The natural frequency dictates the oscillator frequency, dissipation influences the power needs and is intrinsically linked to the resonator noise [4], and nonlinearity limits the acceptable operating vibration amplitude [5]. The latter two directly affect frequency stability through the level of noise (linked to dissipation) and by limiting the signal strength relative to the noise (via stiffness nonlinearity). The nonlinearity converts amplitude noise into frequency noise, the so-called A-F noise conversion, which results in fluctuations in the oscillator period. The design of oscillators for precise and reliable long-term operation involves many engineering challenges, including mechanical design, circuit design, and device packaging.

In terms of fundamental research, various approaches for improving frequency stability (or, equivalently, reducing phase diffusion) may be found in the literature. By analysis of dynamic models, these examine how noise in the oscillator components translates into phase diffusion and finite linewidth. Many of these investigations use an understanding of nonlinearities to tune device parameters and operating conditions to mitigate the effects of noise. These include evasion of amplifier noise by operation at bifurcation points [6, 7], minimizing A-F conversion by using zero-dispersion (ZD) operating points [8–11], use of parametric feedback and nondegenerate parametric drive [12, 13], and other similar effects [14–17]. These approaches are based on oscillator models that use a single mode of vibration of the resonator.

Recent studies have shown that another method for reducing phase diffusion is by coupling the resonator's operational mode in real time to a passive secondary mode in an internal resonance (IR). The first experimental observation of this effect is described in [18], where a 1:3 IR resulted in reduced fluctuations of the oscillator frequency by three orders of magnitude. Subsequently, 1:2 resonances have shown similar beneficial effects [19–21]. The recent paper [22] describes an analytical treatment and experimental validation of a generic model for 1:3 IR with noise that is found to be capable of predicting the observed reductions in phase diffusion by examining the effects of coupling on a slow timescale. The predicted and measured improvements are dramatically below those of a linear resonator running at the corresponding amplitude, thereby exceeding the performance capabilities of single-mode operation. The analysis in [22] reveals that there are two mechanisms behind these improvements. The first mechanism is a consequence of the interaction of the amplitude-dependent frequencies of the modes, which leads to frequency veering in the region where the uncoupled frequencies interact. This results in an amplitude range of significantly reduced dispersion and even the possibility of a ZD amplitude. The second mechanism is related to a modal phase constraint inherent to IR that leads to synchronization of the modes. In this IR synchronization, fluctuations of the first mode are reduced by its phase coupling with the second mode, an effect referred to as phase cleaning [23]. The veering effect is described in detail for 1:2 and 1:3 IR in Ref. [24]. Both effects and experimental validation are analyzed for 1:3 IR in Ref. [22]. Phase cleaning is the only known method for suppressing the effects of multiplicative noise sources beyond their intrinsic single-mode limitation, thus removing a restriction that limits single-mode approaches. It is noteworthy that these two mechanisms are generic for IR and do not require non-monotonic resonator frequency characteristics. However, realizing IR operation in production devices is challenging since it is difficult to maintain the desired frequency mistuning and intermodal coupling in the face of temperature drifts and other environmental effects. So, while the basic idea of mode coupling is appealing, it would be useful to have an alternative approach with similar benefits.

Here, we present an original alternative approach that achieves the equivalent of both reduced dispersion and phase cleaning using a single-mode oscillator with a generic Duffing nonlinearity, i.e., without the need for either specially designed nonlinearities, operation near a bifurcation point, or coupled-mode operation. This is accomplished through the introduction of a secondary control input, acting outside the primary sustaining loop and expressed in terms of an amplitude and phase shift that are made to evolve on the slow timescale of the resonator decay according to user-designed, implementable, adaptive feedback laws. As shown through a linearized analysis of the stochastic dynamics around a steady operating condition found in the deterministic limit, such feedback laws may be designed to reduce and even eliminate phase diffusion to the dominant order of approximation. Among the many advantages over using resonator-based special operating points or internal resonances in coupled-mode resonators, the proposed feedback design may be realized in either hardware (analog) or software (digital) and tuned *a priori* to the desired properties. Notably, the resonator element can be of the generic Duffing type, requiring no special engineering. Also, the secondary loop is not restricted by physics and is, therefore, more flexible in terms of parameter choices, yielding the possibility of improved performance beyond what can otherwise be achieved. As an example, the approach includes a free coupling constant that generalizes the integer ratio between the phases of coupled modes operating near internal resonance. As shown in later sections, the free tuning of this parameter is a useful ingredient in designs that completely eliminate, in an asymptotic limit, phase diffusion of the oscillator.

The remainder of this paper is organized as follows. Section II describes a generic mathematical model for a closed-loop oscillator that includes both the primary sustaining feedback loop and the secondary noise-responsive feedback loop for tailoring the phase response. The method of averaging is used to derive a set of coupled stochastic differential equations that govern the resonator's slowly varying amplitude and phase. An abstract form is then proposed for implementable feedback laws that govern slow variations of two control states that parameterize the amplitude and phase of the secondary control input. This construction relies on a coupling parameter that allows the noisy input to the resonator phase dynamics to also drive the relative phase of the adaptive controller. A discussion on paths to realization demonstrates how the proposed feedback design captures the known effects of operation with passively coupled resonant modes, while also providing opportunities for significant generalization and design flexibility, albeit with additional engineering challenges, e.g., the tracking of the oscillator's phase without an external reference. Section III presents motivating results from numerical simulation of different candidate designs for the adaptive feedback controller, including a design that completely eliminates phase diffusion to dominant order. The numerical results are supported by the rigorous derivation in Sec. IV of closed-form expressions for the corresponding asymptotic diffusion constant for a general class of systems with free-running phase along a limit cycle and specialized to the model at hand. The analytical expression forms the basis for general observations regarding the ability of different design choices to reduce or even eliminate phase diffusion. Finally, the concluding Sec. V summarizes the main findings and points to current work to validate the proposed theory in physical devices.

II. MODEL WITH SECONDARY LOOP

This section describes the adaptive feedback design proposed in this paper to suppress phase diffusion of a self-sustained oscillator subject to frequency and thermal noise, with emphasis on a realization that is *implementable*, i.e., for which the back action may be computed without knowledge of the noise inputs.

A. Model schematic

A typical closed-loop oscillator used for frequency synthesis consists of a resonator element that sets the operating frequency of self-oscillation, and an electronic feedback loop that destabilizes the thermal response and ensures that the energy dissipated by the resonator element is balanced out on average by energy provided by an amplifier, resulting in self-oscillation at a desired amplitude and frequency. A common realization of a closed-loop oscillator uses electronic feedback to drive the resonator synchronously with its oscillation frequency with some preset excitation amplitude and phase shift. A schematic of this is depicted by the resonator and the primary feedback in Fig. 1. The primary feedback includes a phase shift (typically $\pi/2$) and a saturated amplifier gain designed to keep the feedback magnitude constant regardless of the amplitude of the resonator response. This scheme is known as a phase feedback oscillator and is commonly used to suppress one quadrature of the amplifier noise [6, 16, 25, 26].

To suppress phase diffusion, we propose the purposeful addition of a secondary feedback loop, as shown in Fig. 1. This acts similarly to the primary loop in that it drives the resonator synchronously with its oscillation frequency. In contrast to the input from the primary feedback, however, the excitation amplitude T and phase shift θ of the secondary drive signal are not set to fixed values but, instead, vary slowly according to a pair of

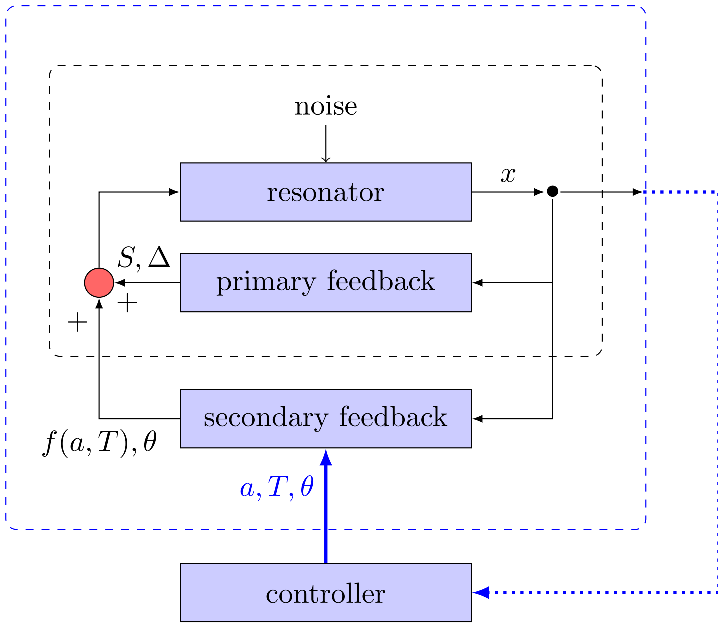

FIG. 1. Schematic block diagram of the closed-loop oscillator with a primary sustaining feedback loop and a proposed secondary feedback loop designed to reduce phase diffusion, i.e., the linear rate of growth with time of the variance of the phase ϕ of the lowest-order dominant contribution $a\cos(\omega t + \phi)$ to the resonator response. In both the primary (inner) and secondary (outer) loops, the oscillator output signal is strongly amplified into diode limiters (with saturation levels S and $f(a,T)$) and phase-shifted (by Δ and θ) to ensure a combined feedback signal of a desired amplitude and relative phase that is used to drive the oscillator and shape its response to noise. While S and Δ have fixed values, the control states T and θ evolve on a slow timescale according to user-designed stochastic adaptive control equations implemented in an external controller. Fig. 2 illustrates the computational algorithm that is implemented in the proposed controller.

appropriately designed stochastic adaptive control equations.

B. Governing equation

As a basic model of the proposed closed-loop oscillator, we consider a single-mode resonator with (i) stiffness nonlinearity that results in frequency pulling, (ii) linear dissipation, (iii) two independent noise sources that act directly on the resonator, namely, thermal (additive) noise and frequency (multiplicative) noise, and (iv) self-sustaining and secondary feedback loops. We let x, $\dot{x}$, and $\ddot{x}$ denote variables that describe the displacement, velocity, and acceleration of the resonator mode. A mathematical model that captures the resonator dynamics in the presence of both the primary and the proposed secondary feedback is then given by the stochastic differential equation

$$\ddot{x} + 2\Gamma\dot{x} + \omega^2(1+\eta(t))x + \gamma x^3 = S\cos(\omega t + \phi + \Delta) + f(a,T)\cos(\omega t + \phi + \theta) + \xi(t) \quad (1)$$

where the parameters Γ, ω, and γ describe the decay rate, eigenfrequency, and cubic stiffness (Duffing/Kerr) nonlinearity, respectively, of the resonator. The frequency and thermal noise terms, denoted here by $\eta(t)$ and $\xi(t)$, respectively, are assumed to be zero-mean, white, Gaussian, delta-correlated, and independent, so that[1] $\langle\eta(t)\rangle = \langle\xi(t)\rangle = \langle\xi(t)\eta(t+h)\rangle = 0$, $\langle\eta(t)\eta(t+h)\rangle = 2\mathcal{I}_\eta\delta(h)$, and $\langle\xi(t)\xi(t+h)\rangle = 2\mathcal{I}_\xi\delta(h)$. In this formulation, we neglect noise from either of the feedback loops (for the self-sustaining feedback loop, this is suppressed, in practice, when $\Delta = \pi/2$ [16]).

The two harmonic terms on the right-hand side of Eq. (1) represent the inputs of the primary and secondary feedback loops on the resonator dynamics. Here,

$$ae^{\mathrm{i}\phi} = \frac{2}{nT_p}\int_{nT_p} x(t)e^{-\mathrm{i}\omega t}\,\mathrm{d}t, \quad (2)$$

where $\int_{nT_p}$ refers to integration over an interval of length $nT_p = 2\pi n/\omega$ for some experimentally convenient integer n (cf. Fig. 2). For slowly varying control signals T and θ and under assumptions made explicit in the next section, this choice is motivated by the lowest-order dominant contributions to the resonator response: $a\cos(\omega t + \phi)$ with slowly varying amplitude a and phase shift ϕ. It is the goal of this paper to show that suitable adaptive design of the variations in $f(a,T)$ and θ over the slow timescale can modify the resonator response to noise-induced fluctuations in desirable ways.

To model the dominant dynamics of interest, we assume that the model in Eq. (1) experiences slow decay compared to its oscillation timescale ($\Gamma \ll \omega$) and, therefore, requires only weak drive to maintain self-oscillation ($|S| \ll \omega^2|x|$). It is also assumed to operate with weak nonlinearity ($|\gamma x^2| \ll \omega^2$) and to be subjected to small-intensity noise (as defined in the sequel). In addition, the secondary drive is assumed to be small ($|f(a,T)| \ll \omega^2|x|$).

[1] Here, $\langle g(t)\rangle$ denotes the time average of $g(t)$, which is equal to the ensemble average over realizations for ergodic processes. This idealization of the noise terms can also be used for general stationary, zero-mean, non-Gaussian processes, as long as their correlation times are considerably shorter than the relaxation time of the resonator [27], i.e., for $\tau_{\mathrm{cor}} = \langle\xi^2\rangle^{-1}\int_0^\infty\langle\xi(t))\xi(t+h)\rangle\,\mathrm{d}h \ll 1/\Gamma$.

Motivated by these assumptions, we define the non-dimensional scaling parameter $\varepsilon = \Gamma/\omega$ and let $x(t) = y(\omega t)$ to obtain the equation

$$y'' + y = \varepsilon \left(S\cos(\tau+\phi+\Delta) + f(a,T)\cos(\tau+\phi+\theta) - 2y' - \gamma y^3\right) + \sqrt{\varepsilon}(\xi - \eta y). \qquad (3)$$

Here, $'$ denotes differentiation with respect to $\tau = \omega t$ and we have substituted $\gamma \mapsto \varepsilon\omega^2\gamma$, $S \mapsto \varepsilon\omega^2 S$, $f(a,T) \mapsto \varepsilon\omega^2 f(a,T)$, $\xi(t) \mapsto \sqrt{\varepsilon}\omega^2\xi(\tau)$, $\eta(t) \mapsto \sqrt{\varepsilon}\eta(\tau)$ (such that $\mathcal{I}_\xi \mapsto \varepsilon\omega^3\mathcal{I}_\xi$ and $\mathcal{I}_\eta \mapsto \varepsilon\omega^{-1}\mathcal{I}_\eta$), and

$$ae^{\mathrm{i}\phi} = \frac{1}{\pi n}\int_{2\pi n} y(\tau)e^{-\mathrm{i}\tau}\,\mathrm{d}\tau, \qquad (4)$$

where $\int_{2\pi n}$ refers to integration over an interval of length $2\pi n$.

For $\varepsilon \ll 1$, while the resonator exhibits fast oscillations with frequency 1, its amplitude a and phase ϕ and, by design, the control signals T and θ, are slowly-varying and effectively constant over the fast timescale. We make this explicit in the following section using the method of stochastic averaging [27].

C. Amplitude and phase dynamics

To capture the slow amplitude and phase dynamics assuming $\varepsilon \ll 1$ and consistent with Eq. (4), we define the slowly varying stochastic processes $a(\varepsilon\tau)$ and $\phi(\varepsilon\tau)$ by the equalities

$$y(\tau) = a(\varepsilon\tau)\cos(\tau + \phi(\varepsilon\tau)),\ y'(\tau) = -a(\varepsilon\tau)\sin(\tau+\phi(\varepsilon\tau)) \qquad (5)$$

such that, by construction,

$$a'\cos(\tau+\phi) - a\phi'\sin(\tau+\phi) = 0. \qquad (6)$$

Substitution of Eq. (5) into Eq. (3) and Gauss elimination using Eq. (6) then yields

$$a' = f_a(a,T,\theta) - \xi\sin(\tau+\phi) + \frac{1}{2}\eta\, a\sin\left(2\tau+2\phi\right), \qquad (7)$$

$$\phi' = f_\phi(a,T,\theta) - \frac{\xi}{a}\cos(\tau+\phi) + \eta\cos^2(\tau+\phi), \qquad (8)$$

where differentiation is with respect to the slow time variable $s = \varepsilon\tau = \Gamma t$,

$$f_a(a,T,\theta) = -a + \frac{S\sin\Delta + f(a,T)\sin\theta}{2}, \qquad (9)$$

$$f_\phi(a,T,\theta) = \frac{3\gamma a^2}{8} - \frac{S\cos\Delta + f(a,T)\cos\theta}{2a}, \qquad (10)$$

we have substituted $\xi(\tau) \mapsto \sqrt{\varepsilon}\xi(s)$ and $\eta(\tau) \mapsto \sqrt{\varepsilon}\eta(s)$, and we have neglected oscillatory terms on the right-hand sides of Eqs. (7) and (8) that average to zero on the fast timescale. Then, following Section 7.2 of [27], for sufficiently small ε and to lowest order in ε, the stochastic processes a and ϕ can be approximately modeled by Markov processes on the slow timescale governed by the equations

$$a' = f_a(a, T, \theta) + \sqrt{I_a(a)}\,\chi_1(s), \tag{11}$$

$$\phi' = f_\phi(a, T, \theta) + \sqrt{I_\phi(a)}\,\chi_2(s), \tag{12}$$

where (see the appendix for a derivation)

$$I_a(a) = \frac{a^2\mathcal{I}_\eta}{4} + \mathcal{I}_\xi,\ \ I_\phi(a) = \frac{3\mathcal{I}_\eta}{4} + \frac{\mathcal{I}_\xi}{a^2}, \tag{13}$$

and χ_1 and χ_2 are delta-correlated random processes with means $\langle\chi_i(s)\rangle = 0$ and correlations $\langle\chi_i(s)\chi_j(s+\sigma)\rangle = \delta_{ij}\delta(\sigma)$.

It is important to note that neither f_a nor f_ϕ depend on the free-running phase ϕ. This quality is innate for self-oscillation and critical for both the design of the proposed feedback architecture and its theoretical analysis.

D. Feedback design

The expressions for f_a and f_ϕ in Eqs. (9) and (10) suggest an opportunity to regulate the noise-perturbed dynamics of $a(\varepsilon\tau)$ and $\phi(\varepsilon\tau)$ by suitable (slow) time variations of $T(\varepsilon\tau)$ and $\theta(\varepsilon\tau)$. We propose realizing such time variations by engineering dynamics that result in adaptive Langevin equations of the particular form

$$T' = f_T(a, T, \theta), \tag{14}$$

$$\theta' = f_\theta(a, T, \theta) + k\sqrt{I_\phi(a)}\chi_2(s) \tag{15}$$

for some user-defined functions f_T and f_θ and user-selected scalar constant k. Consistent with the forms of f_a and f_ϕ, neither f_T nor f_θ depend on ϕ. Moreover, a nonzero value of k implies that the noise input driving θ is a scaled version of the noise input driving ϕ. Such coupling with k fixed by the physics of an internal resonance has been shown to allow coupled-mode oscillators to achieve significant reductions in phase diffusion [22]. At will selection of k without reference to any inherent physics, coupled with the design of f_T, f_θ

(and the amplitude factor $f(a,T)$), provides a rich opportunity for the adaptive feedback to respond to noise-driven fluctuations in the phase dynamics. Indeed, as shown in later sections, a suitable adaptive feedback design can *completely eliminate* phase diffusion to leading order. As of yet, this level of frequency stability has not been found achievable using properties such as zero dispersion points or internal resonance.

Since Eq. (14) lacks an explicit noise term, it is *implementable*, e.g., in a computer simulation that runs in parallel to the oscillator dynamics, provided that one has access to measurable values of a, T, and θ. In contrast, by the very nature of noise, the explicit noise term in Eq. (15) makes this equation *unimplementable*. By design, however, the coupled phase variable $\psi = \theta - k\phi$ must satisfy the Langevin equation

$$\psi' = f_\theta(a, T, \theta) - k f_\phi(a, T, \theta), \tag{16}$$

which is implementable. Provided that a and ϕ are measurable, both T and $\theta = \psi + k\phi$ are measurable, and the desired dynamics for T and θ may be realized using implementable real-time computations.

The closed-loop system dynamics may thus be understood either in terms of the state (a, ϕ, T, ψ) and Langevin equations (11), (12), (14), and (16) with $\theta = \psi + k\phi$ or, equivalently, in terms of the state (a, ϕ, T, θ) and Langevin equations (11), (12), (14), and (15). While the former represents an actual implementation in which (a, ϕ) are obtained from the resonator response and (T, ψ) are integrated numerically (as also illustrated in Fig. 2), the latter formulation is particularly useful for the theoretical analysis in Sec. IV.

E. Paths to realization

As shown in the previous sections, the proposed secondary feedback loop acts directly on the resonator on the fast timescale but with control parameters that are regulated only on the slow timescale. This reflects the fact that while phase diffusion manifests itself primarily on the slower timescale, control actuation must be realized in real time. With this in mind, we recognize two paths to realizing the feedback laws (14) and (16) and discuss these in some detail here.

According to the first path, feedback laws (14) and (16) are the result of real-time physical interactions that, when averaged over the fast timescale, yield slowly-varying quantities T

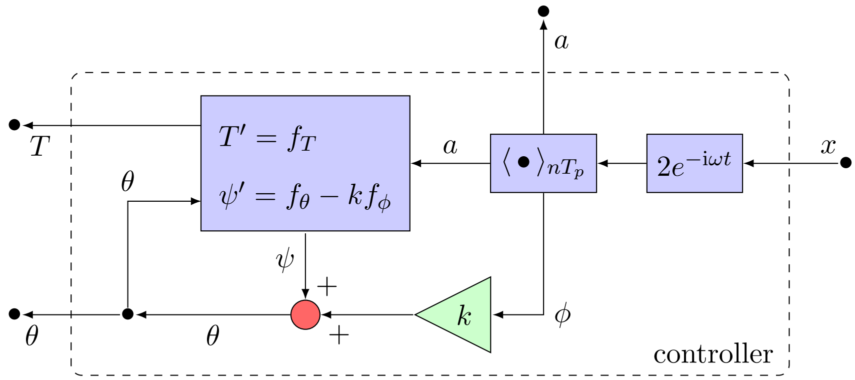

FIG. 2. Schematic block diagram of the algorithm implemented in the controller block of Fig. 1. Here, the two rightmost operator blocks implement Eq. (2), while the adaptive updates to T and ψ in the leftmost block implement the feedback design in Eqs. (14) and (16). The latter are expressed in terms of the designable functions f_T and f_θ and the model function f_ϕ, all of which depend on a, T, and $\theta = \psi + k\phi$.

and θ that satisfy stochastic differential equations of the form (14) and (15) without any manual intervention.

For example, for two passively-coupled vibration modes in approximately 1:2 resonance, i.e., with natural frequencies ω_1 and $\omega_2 = 2\omega_1 - \varepsilon\Delta\omega$ where $\varepsilon = \Gamma_1/\omega_1 \ll 1$, the slow amplitude and phase dynamics may be modeled in the limit of small noise by

$$a_1' = -a_1 + \frac{\alpha a_1 a_2 \sin\varphi}{4} + \frac{S\sin\Delta}{2} + \sqrt{I_{a_1}(a_1)}\,\chi_1(s), \tag{17a}$$

$$\phi_1' = \frac{1}{4}\left(\frac{3\gamma a_1^2}{2} + \alpha a_2\cos\varphi - \frac{2S\cos\Delta}{a_1}\right) + \sqrt{I_{\phi_1}(a_1)}\,\chi_2(s), \tag{17b}$$

$$a_2' = -\frac{\Gamma_2}{\Gamma_1}a_2 - \frac{\alpha a_1^2\sin\varphi}{8}, \tag{17c}$$

$$\varphi' = \frac{\Delta\omega}{\omega_1} + \frac{1}{2}\left(\frac{3\gamma a_1^2}{2} + \alpha a_2\cos\varphi - \frac{2S\cos\Delta}{a_1}\right) - \frac{\alpha a_1^2\cos\varphi}{8a_2} + 2\sqrt{I_{\phi_1}(a_1)}\,\chi_2(s), \tag{17d}$$

where $\varphi = 2\phi_1 - \phi_2$, α is the inter-modal coupling parameter from the single-term interaction potential of the 1:2 internal resonance [28], i.e., $U_{\mathrm{cpl}} = \alpha x_1^2 x_2$, and the subscripts 1 and 2 refer to various quantities of the first and second mode, respectively. We recover Eqs. (11), (12), (14), and (15) by identifying $a = a_1$, $\phi = \phi_1$, $T = a_2$, and $\theta = -\varphi$, and letting

$f(a,T) = -\alpha a T/2$, $k=-2$, and

$$f_T = -\frac{\Gamma_2}{\Gamma_1}T + \frac{\alpha a^2 \sin\theta}{8}, \tag{18}$$

$$f_\theta = -\frac{\Delta\omega}{\omega_1} - \frac{1}{2}\left(\frac{3\gamma a^2}{2} + \alpha T\cos\theta - \frac{2S\cos\Delta}{a}\right) + \frac{\alpha a^2\cos\theta}{8T}. \tag{19}$$

For this resonance, experimental observations of improved frequency stability below the noise levels of single-mode oscillators have been documented in the literature [19–21].

Similar observations apply to the equations modeling two passively-coupled modes with an approximate 1:3 internal resonance, which experimentally showed three orders of magnitude improvement in frequency stability when operated in resonance [18], results that were analyzed and explained in [22] in terms of reduced dispersion and phase cleaning. In the limit of small noise, the corresponding amplitude and phase dynamics are modeled by

$$a_1' = -a_1 + \frac{3\alpha a_1^2 a_2 \sin\varphi}{8} + \frac{S\sin\Delta}{2} + \sqrt{I_{a_1}(a_1)}\,\chi_1(s), \tag{20a}$$

$$\phi_1' = \frac{1}{4}\left(\frac{3\gamma a_1^2}{2} + \frac{3\alpha a_1 a_2\cos\varphi}{2} - \frac{2S\cos\Delta}{a_1}\right) + \sqrt{I_{\phi_1}(a_1)}\,\chi_2(s), \tag{20b}$$

$$a_2' = -\frac{\Gamma_2}{\Gamma_1}a_2 - \frac{\alpha a_1^3\sin\varphi}{24}, \tag{20c}$$

$$\varphi' = \frac{\Delta\omega}{\omega_1} + \frac{3}{4}\left(\frac{3\gamma a_1^2}{2} + \frac{3\alpha a_1 a_2\cos\varphi}{2} - \frac{2S\cos\Delta}{a_1}\right) - \frac{\alpha a_1^3\cos\varphi}{24 a_2} + 3\sqrt{I_{\phi_1}(a_1)}\,\chi_2(s), \tag{20d}$$

where $\varphi = 3\phi_1 - \phi_2$, $\varepsilon\Delta\omega = 3\omega_1 - \omega_2$, $\varepsilon = \Gamma_1/\omega_1$, and α is the inter-modal coupling parameter from the single-term interaction potential of the 1:3 internal resonance [23], i.e., $U_{\mathrm{cpl}} = \alpha x_1^3 x_2$. In this case, we recover Eqs. (11), (12), (14), and (15) by identifying $a = a_1$, $\phi = \phi_1$, $T = a_2$, and $\theta = -\varphi$, and letting $f(a,T) = -3\alpha a^2 T/4$, $k=-3$, and

$$f_T = -\frac{\Gamma_2}{\Gamma_1}T + \frac{\alpha a^3\sin\theta}{24}, \tag{21}$$

$$f_\theta = -\frac{\Delta\omega}{\omega_1} - \frac{3}{4}\left(\frac{3\gamma a^2}{2} + \frac{3\alpha a T\cos\theta}{2} - \frac{2S\cos\Delta}{a}\right) + \frac{\alpha a^3\cos\theta}{24T}. \tag{22}$$

In both of these examples, the value of k is not selectable at will, but instead constrained by the resonance. The forms of f_T and f_θ are likewise constrained by the nature of the physical coupling, albeit with the potential for tuning the inter-modal coupling parameter α to reduce phase diffusion at a desired operating amplitude. We surmise the possibility that other forms of physical coupling, including with nonlinear active elements rather than purely passive coupling, can provide additional design flexibility and opportunities for optimal tuning, but are not aware of such work to date.

According to the second path, on the other hand, feedback laws (14) and (16) are implemented *algorithmically* only on the slow timescale, while the action of the secondary feedback loop is exactly as shown in Figs. 1 and 2 and modeled in (1), without any further physical coupling.

As discussed in conjunction with (16), feedback according to this second path requires tracking the slowly-varying amplitude and phase of the oscillator. While the amplitude is readily measured, estimation of the phase poses a greater challenge, as this typically requires demodulation with a reference oscillator that is cleaner than the oscillator of interest. But if such a reference oscillator is readily available, why bother transferring its frequency stability to the resonator at hand? Self-referencing demodulation against a time-delayed version of the oscillator's own response [29, 30] may offer an alternative to the use of such an external reference.

Compared to the realization according to the first path, the algorithmic implementation operates using only a single resonator mode, eliminating the need for careful device engineering as is necessary for the case of zero dispersion or internal resonance. Moreover, whereas resonance is associated with integer values of k ($= -n$ for $1{:}n$ internal resonance), here the value of k may be set arbitrarily and thus optimized to achieve desired performance. Finally, while internal resonance may produce favorable noise suppression characteristics near critical operating amplitudes, the secondary feedback parameters may be freely designed to achieve such behavior near any amplitude.

Following either path, the analysis in later sections assumes that no additional effects of noise are introduced in (14) and (16). Indeed, in the derivation of (17a-17d) and (20a-20d), it was assumed *a priori* that the stochastic terms need only account for the effects of the primary feedback loop, rather than uncertainty inherent in each oscillatory mode. Similarly, in the algorithmic realization, it is assumed *a priori* that no additional uncertainty arises due to the secondary feedback loop, including as a result of phase demodulation against a time-delayed signal. We briefly reiterate these assumptions in the concluding section.

III. NUMERICAL SIMULATIONS

To motivate the detailed analysis in the next section, as well as to provide data against which this analysis may be compared, we present here the results of numerical simulations of the nonlinear coupled stochastic differential equations given by Eqs. (11), (12), (14), and (15) for several choices of feedback design and near operating conditions that correspond to steady-state dynamics in the deterministic limit, i.e., $(a, T, \theta) = (a_{\mathrm{ss}}, T_{\mathrm{ss}}, \theta_{\mathrm{ss}})$ such that $f_a = f_T = f_\theta = 0$. We note that without the secondary loop ($f(a, T) = 0$) the deterministic operating condition has amplitude $a_{\mathrm{ss}} = S \sin \Delta/2$. Our focus is on control designs that maintain this steady operating condition, albeit with different dynamics.

Since we are concerned only with noise-induced perturbations near a deterministic steady-state limit, we restrict attention to feedback designs for which f_T and f_θ are linear in the deviations of a, T, and θ from their steady-state values, i.e.,

$$f_T(a, T, \theta) = G_{aT}(a - a_{\mathrm{ss}}) + G_{TT}(T - T_{\mathrm{ss}}) + G_{\theta T}(\theta - \theta_{\mathrm{ss}}), \tag{23}$$

$$f_\theta(a, T, \theta) = G_{a\theta}(a - a_{\mathrm{ss}}) + G_{T\theta}(T - T_{\mathrm{ss}}) + G_{\theta\theta}(\theta - \theta_{\mathrm{ss}}). \tag{24}$$

We fix the self-sustaining feedback parameters[2] at $S = 3$ and $\Delta = \pi/2$, the cubic nonlinearity at $\gamma = 1$, and the thermal and frequency noise intensities at $\mathcal{I}_\xi = \mathcal{I}_\eta = 10^{-4}$. We restrict attention to designs with $f(a, T) = -T$ and $\theta_{\mathrm{ss}} = 0$, from which it follows that $a_{\mathrm{ss}} = S \sin \Delta/2 = 3/2$, $I_a(a_{\mathrm{ss}}) = 1/6400$, and $I_\phi(a_{\mathrm{ss}}) = 43/360000$.

To quantify the simulation results and compare them with the theory developed below, we focus on the statistics of the phase ϕ. Of primary interest is the asymptotic phase diffusion, which we expect to be dominated by a linear growth of the phase variance $\langle \phi^2(s) \rangle - \langle \phi(s) \rangle^2 \sim \mathrm{D}_\phi s$ provided that the corresponding asymptotic phase diffusion constant D_ϕ is nonzero. It can be shown that in the case of small and confined amplitude fluctuations and small diffusion constant relative to the eigenfrequency ($\mathrm{D}_\phi \ll 1$), the diffusion coefficient D_ϕ represents the linewidth of the oscillator output. This provides a convenient connection between our theoretical predictions and a commonly measured quantity describing the frequency stability of an oscillator [22, 31, 32].

We simulated the resultant stochastic dynamics for three different designs of the secondary loop characterized by select choices of gain parameters G_{**}, phase coupling constant k, and steady-state value T_{ss}. Brief descriptions of these controllers is provided, but the details of their selection requires the analysis in the subsequent sections. The control parameters and descriptions are as follows:

[2] The value $\Delta = \pi/2$ maximizes the value of a_{ss}, which in turn minimizes the contribution to $I_\phi(a_{\mathrm{ss}})$ from thermal noise as seen in Eq. (13). Normally, the optimal operating amplitude occurs where this beneficial large amplitude effect is countered by the increased phase diffusion from amplitude-to-frequency conversion.

(i) $G_{aT} = G_{\theta T} = G_{a\theta} = G_{T\theta} = 0$, $G_{TT} = G_{\theta\theta} = -1$, $k = 0$, and $T_{\text{ss}} \in [1, 10]$. This control simply drives $T \to T_{\text{ss}}$ and $\theta \to 0$. For $T_{\text{ss}} = 0$, the asymptotic dynamics corresponds to the absence of the secondary loop and replicates the response of a standard oscillator with resonator Duffing nonlinearity, a result used for baseline reference.

(ii) $G_{\theta T} = G_{\theta\theta} = 0$, $2G_{aT} = -2G_{TT} = 2G_{a\theta} = G_{T\theta} = 2$, $k = 0$, and $T_{\text{ss}} \in [1, 10]$. As described in Section IV, this control eliminates effects analogous to amplitude-to-frequency conversion but does not utilize phase coupling since $k = 0$.

(iii) $G_{\theta T} = G_{\theta\theta} = 0$, $2G_{aT} = -2G_{TT} = 2G_{a\theta} = G_{T\theta} = 2$, $k \in [0, 5]$, and $T_{\text{ss}} = 1$. As described in Section IV, this control eliminates effects analogous to amplitude-to-frequency conversion and also utilizes phase coupling.

To produce the results reported below, we used the Euler–Maruyama method [33] with a constant time-step of $\Delta s = 10^{-4}$ for $N = \lfloor s_{\max}/\Delta s \rfloor$ time-steps, i.e., for $s \in [0, s_{\max}]$. For ensemble statistics, we collected the results of $M = 10^3$ simulations. In each case, we emphasize the time-dependence of the phase variance $\langle \phi^2(s) \rangle - \langle \phi(s) \rangle^2$ and characterize as phase diffusion an approximately linear asymptotic growth of this quantity with s.

Fig. 3 shows the results of numerical simulations of the fully nonlinear slow equations for (a, ϕ, T, θ) for feedback designs of type (i) with $T_{\text{ss}} = 0$, (ii) with $T_{\text{ss}} = 1$, and (iii) with $k = 216/89$, respectively. The results shown in the upper panel reveal that the phase variances for feedback designs (i) and (ii) increase approximately linearly in time while the phase variance for feedback design (iii) appears to be approach a finite bound $\text{dc} \approx 3.8 \times 10^{-4}$ without any asymptotic linear growth. The time histories match closely to the dashed lines in the figure obtained using a closed-form expression for the diffusion constant D_ϕ that is derived in Sec. IV. Indeed, in the case of feedback design (iii), the theory predicts $\text{D}_\phi = 0$, which is certainly consistent with the observed absence of asymptotic linear growth. As shown in the lower panels, the phase distribution when scaled by $\sqrt{s}$ is in all cases Gaussian, consistent with the use in Sec. IV of a linearized theory, as both the input and output of the dynamical system are Gaussian.

The boundedness of the phase variance for feedback design type (iii) implies near-ideal long-term frequency stability, since the corresponding line width scales as $\text{dc}/s_{\max}$. Therefore, as we increase $s_{\max}$, the phase distribution becomes more narrowly peaked (Fig. 4).

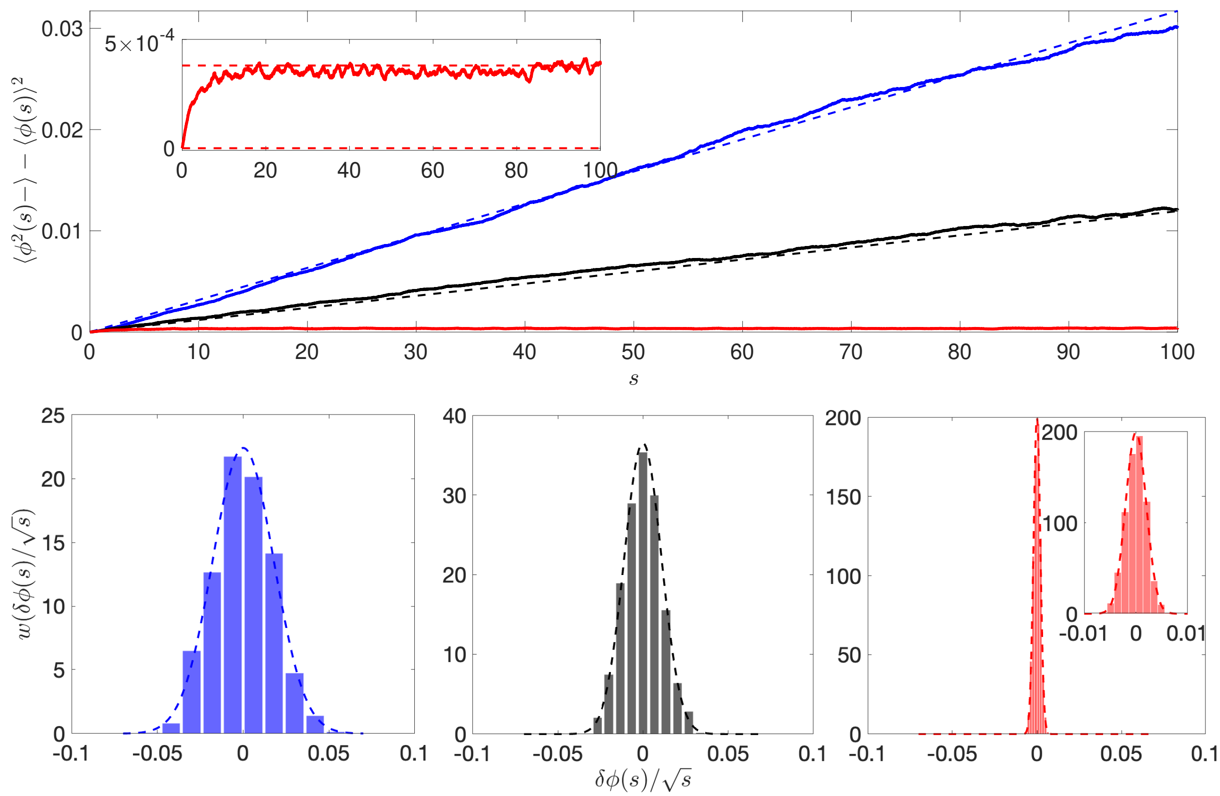

FIG. 3. Numerical simulations and theoretical predictions of phase diffusion for feedback design (i) with $T_{\rm ss} = 0$ (blue), (ii) with $T_{\rm ss} = 1$ (black), and (iii) with $k = 216/89$ (red). The upper panel shows the phase variance as a function of time along with straight lines representing the asymptotically linear trends predicted using a linearized theory in Sec. IV. The inset in the upper panel shows a zoomed-in view of the phase variance for feedback design (iii) showing asymptotic growth to a finite bound dc $= 3.8 \times 10^{-4}$. The lower panels show the distribution for 10^3 samples of the deviation $\delta\phi(s) = \phi(s) - \langle\phi(s)\rangle$ of the phase at $s = 100$ (i.e., after 10^6 time-steps) from its mean, normalized by $\sqrt{s}$.

This path toward the delta function distribution of an ideal oscillator is limited by our assumptions and the stochastic analysis that considers only the short-term frequency stability of the oscillator. In practice, when increasing the integration time, long time-scale effects, such as aging and $1/f$ noise processes, which are not accounted for in our analysis, will become dominant and control the long-term frequency stability [2].

We collect the estimated diffusion constants from numerical simulations of the fully nonlinear slow equations for (a, ϕ, T, θ) for feedback designs types (i)-(iii) across the indicated

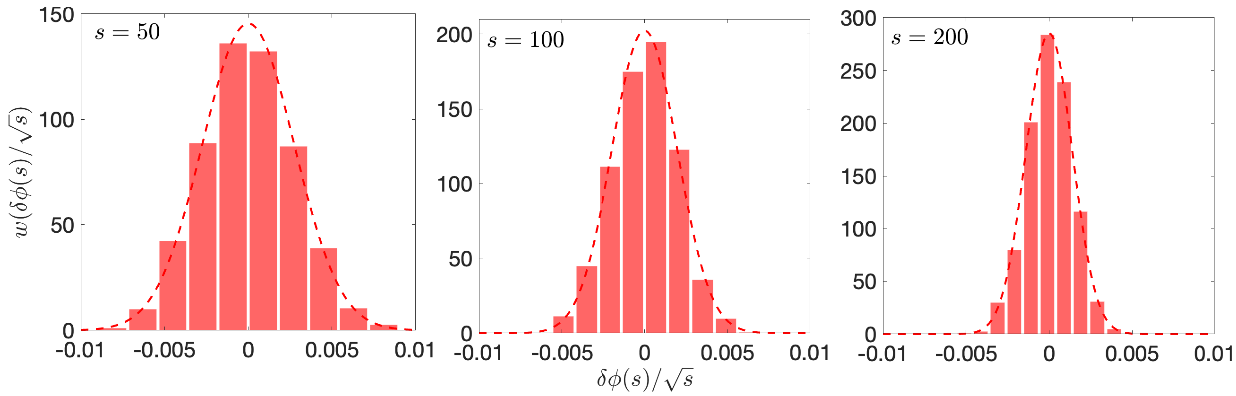

FIG. 4. Numerical simulations and theoretical predictions of the phase distribution around the mean phase for feedback design (iii) at $s = 50$ (left), $s = 100$ (middle), and $s = 200$ (right). The theoretical predictions (dashed curves) are zero-mean Gaussian distributions with variance $\mathrm{d}c/s$.

ranges of T_{ss} and k in Fig. 5. Theoretical predictions, based on the linearized stochastic equations derived in Sec. IV, are shown for comparison. Interestingly, while for feedback design (i), the diffusion constant depends apparently quadratically on T_{ss}, it is independent of T_{ss} for feedback design (ii) and apparently equal to the minimum value observed for feedback design (i). This operating condition is the best that can be achieved using this controller and corresponds to the baseline reference in the absence of the secondary loop. In contrast, for feedback design (iii), we observe a quadratic dependence on k that appears to achieve its minimum at $\mathrm{D}_\phi = 0$ for $k \approx 2.4$ consistent with the theoretical prediction of 216/89.

As suggested by the figures in this section, an asymptotic theory is available to compute the diffusion constant in terms of the given model and adaptive gain parameters. We turn to this theory next and use the results to support a purposeful selection of gain parameters that optimally enhance frequency stability in the asymptotic limit.

IV. THEORETICAL ANALYSIS

The results in the previous section show that, after a brief initial transient, the phase variance typically grows linearly in time, described by the form $\langle \phi^2(s)\rangle - \langle \phi(s)\rangle^2 \sim \mathrm{D}_\phi s$, where the rate D_ϕ is the diffusion coefficient, the key quantity used in our analysis to measure the frequency stability of the oscillator. In this section, we use an asymptotic linearized analysis of the stochastic system near the deterministic steady-state condition to derive a

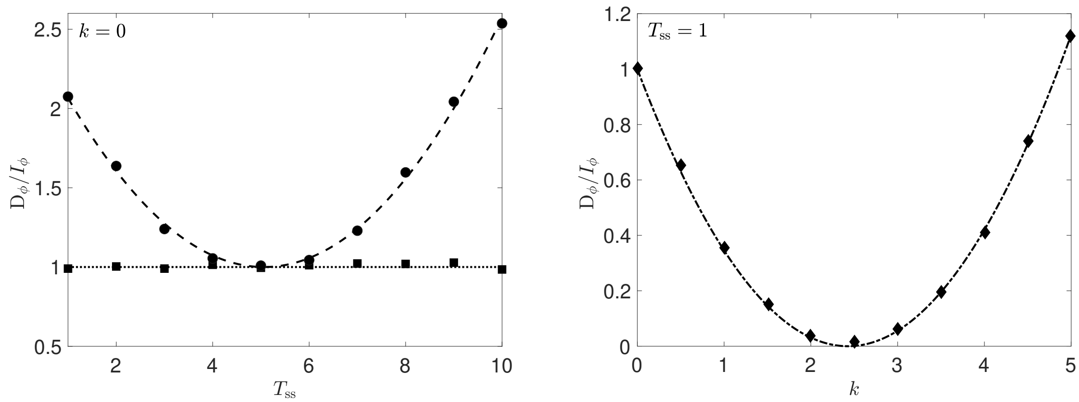

FIG. 5. Numerical simulations and theoretical predictions (from Sec. IV) of the normalized phase diffusion $\mathrm{D}_\phi/I_\phi(a_{\mathrm{ss}})$ for feedback designs (i)-(iii). Left panel: the black dots and dashed curve correspond to variations in T_{ss} for design (i), while the black squares and dotted curve correspond to variations in T_{ss} for design (ii). Right panel: the black diamonds and dashed-dotted curve correspond to variations in k for design (iii).

closed-form prediction for the corresponding asymptotic diffusion coefficient. We use the resulting expression to guide the feedback design and to explain the numerical observations. In particular, we find a class of feedback designs for which the predicted asymptotic diffusion constant equals zero.

A. Asymptotic phase diffusion

Let (a, T, θ, ϕ) denote the slowly varying state of the closed-loop dynamics in Sec. II. Then, if we ignore the small drift terms in Eq. (11), we obtain the governing state-space dynamics

$$\begin{pmatrix} a' \\ T' \\ \theta' \\ \phi' \end{pmatrix} = \begin{pmatrix} f_a(a, T, \theta) \\ f_T(a, T, \theta) \\ f_\theta(a, T, \theta) \\ f_\phi(a, T, \theta) \end{pmatrix} + \boldsymbol{B}\sqrt{\boldsymbol{I}_{\boldsymbol{\chi}}(a)}\boldsymbol{\chi}(s), \tag{25}$$

where

$$\boldsymbol{B}=\begin{pmatrix}1&0\\0&0\\0&k\\0&1\end{pmatrix},\ \sqrt{\boldsymbol{I}_{\boldsymbol{\chi}}(a)}=\begin{pmatrix}\sqrt{I_a(a)}&0\\0&\sqrt{I_\phi(a)}\end{pmatrix},\ \boldsymbol{\chi}(t)=\begin{pmatrix}\chi_1(s)\\\chi_2(s)\end{pmatrix},\tag{26}$$

and, as advertised, the right-hand sides are notably independent of ϕ. When $\chi_1(s)=\chi_2(s)\equiv 0$, we define a steady oscillatory state by a condition $(a,T,\theta)=(a_{\mathrm{ss}},T_{\mathrm{ss}},\theta_{\mathrm{ss}})$, such that $f_a(a_{\mathrm{ss}},T_{\mathrm{ss}},\theta_{\mathrm{ss}})=f_T(a_{\mathrm{ss}},T_{\mathrm{ss}},\theta_{\mathrm{ss}})=f_\theta(a_{\mathrm{ss}},T_{\mathrm{ss}},\theta_{\mathrm{ss}})=0$, and a constantly rotating phase with $\phi'=\phi'_{\mathrm{ss}}:=f_\phi(a_{\mathrm{ss}},T_{\mathrm{ss}},\theta_{\mathrm{ss}})$, such that the noise-free oscillator frequency equals $\Omega=1+\varepsilon\phi'_{\mathrm{ss}}$. We assume that this steady state is locally exponentially stable, i.e., that the eigenvalues of the Jacobian matrix of $(f_a,f_T,f_\theta)^\mathsf{T}$ with respect to (a,T,θ) and evaluated at $(a_{\mathrm{ss}},T_{\mathrm{ss}},\theta_{\mathrm{ss}})$ have negative real parts.

In the presence of sufficiently weak noise, we expect (a,T,θ) to fluctuate near their steady-state values and are interested in the effects of such fluctuations on the dynamics in the phase ϕ. To analyze this situation, we linearize Eq. (25) around the steady oscillatory state and obtain a set of linear stochastic equations of the form

$$\boldsymbol{v}'=\boldsymbol{A}\boldsymbol{v}+\boldsymbol{B}\sqrt{\boldsymbol{I}_{\boldsymbol{\chi}}(a_{\mathrm{ss}})}\boldsymbol{\chi}(s),\ \boldsymbol{v}=\begin{pmatrix}\delta\boldsymbol{u}\\\delta\phi\end{pmatrix},\ \boldsymbol{A}=\begin{pmatrix}\boldsymbol{J}&\boldsymbol{0}\\\boldsymbol{g}^\mathsf{T}&0\end{pmatrix},\tag{27}$$

where $\delta\boldsymbol{u}=(a-a_{\mathrm{ss}},T-T_{\mathrm{ss}},\theta-\theta_{\mathrm{ss}})^\mathsf{T}$ and $\delta\phi=\phi-\phi_0-\phi'_{\mathrm{ss}}s$ for some constant ϕ_0. Here, $\boldsymbol{J}$ is the aforementioned Jacobian matrix while the components of the row vector $\boldsymbol{g}^\mathsf{T}$ are the partial derivatives of f_ϕ with respect to (a,T,θ) evaluated at $(a_{\mathrm{ss}},T_{\mathrm{ss}},\theta_{\mathrm{ss}})$.

A key result that is relied upon repeatedly in the sequel is the prediction of a diffusion constant that describes the rate of asymptotic linear growth with time s of the variance of the scalar phase variable $\delta\phi$ in Eq. (27). By the assumption on the eigenvalues of $\boldsymbol{J}$, and for a noise vector $\boldsymbol{\chi}(s)$ that is zero-mean and delta-correlated (i.e., $\langle\boldsymbol{\chi}(s)\rangle=0$ and $\langle\chi_i(s)\chi_j(s+\sigma)\rangle=\delta_{ij}\delta(\sigma)$), the first two moments of $\boldsymbol{v}$ are given by

$$\langle\boldsymbol{v}(s)\rangle=e^{s\boldsymbol{A}}\boldsymbol{v}(0)\tag{28}$$

and

$$\left\langle(\boldsymbol{v}(s)-\langle\boldsymbol{v}(s)\rangle)(\boldsymbol{v}(s)-\langle\boldsymbol{v}(s)\rangle)^\mathsf{T}\right\rangle=\int_0^s e^{s'\boldsymbol{A}}\boldsymbol{B}\boldsymbol{I}_{\boldsymbol{\chi}}(a_{\mathrm{ss}})\boldsymbol{B}^\mathsf{T}e^{s'\boldsymbol{A}^\mathsf{T}}\,\mathrm{d}s',\tag{29}$$

where the matrix exponential

$$e^{s\boldsymbol{A}} = \begin{pmatrix} e^{s\boldsymbol{J}} & \boldsymbol{0} \\ \boldsymbol{g}^\top \boldsymbol{J}^{-1}(e^{s\boldsymbol{J}} - \boldsymbol{I}) & 1 \end{pmatrix} \tag{30}$$

has entries that are either constant or converge exponentially fast to constants. In particular, the asymptotic values of the right-hand side of Eq. (28) may be determined by letting $e^{s\boldsymbol{J}} \to 0$, from which it follows that $\langle \delta\boldsymbol{u}(s)\rangle \to 0$ and that $\langle \delta\phi(s)\rangle$ converges to a constant.

Similarly, the entries on the right-hand side of Eq. (29) converge exponentially fast to functions that grow linearly in time at a rate that may be determined by letting $e^{s\boldsymbol{J}} \to 0$ in the expression for $e^{s\boldsymbol{A}}$ and evaluating the integrand. In terms of the notation

$$\boldsymbol{B}\boldsymbol{I}_{\boldsymbol{\chi}}(a_{\mathrm{ss}})\boldsymbol{B}^\top = \begin{pmatrix} \boldsymbol{B}_u & \boldsymbol{b} \\ \boldsymbol{b}^\top & B_l \end{pmatrix}, \tag{31}$$

these asymptotic rates of linear growth are given by the entries of

$$e^{s\boldsymbol{A}}\boldsymbol{B}\boldsymbol{I}_{\boldsymbol{\chi}}(a_{\mathrm{ss}})\boldsymbol{B}^\top e^{s\boldsymbol{A}^\top} \sim \begin{pmatrix} \boldsymbol{0} & \boldsymbol{0} \\ 0 & \boldsymbol{g}^\top \boldsymbol{J}^{-1}\boldsymbol{B}_u \boldsymbol{J}^{-1,\top}\boldsymbol{g} - 2\boldsymbol{b}^\top \boldsymbol{J}^{-1,\top}\boldsymbol{g} + B_l \end{pmatrix}. \tag{32}$$

The non-trivial entry corresponds to the advertised rate of asymptotic linear growth with s of the variance of $\delta\phi(s)$. Therefore, we conclude that

$$\mathrm{D}_\phi = \boldsymbol{g}^\top \boldsymbol{J}^{-1}\boldsymbol{B}_u \boldsymbol{J}^{-1,\top}\boldsymbol{g} - 2\boldsymbol{b}^\top \boldsymbol{J}^{-1,\top}\boldsymbol{g} + B_l \tag{33}$$

is the corresponding asymptotic diffusion constant, the quantity of principal interest. This is linear in the diagonal entries of $\boldsymbol{I}_{\boldsymbol{\chi}}$.

From Eq. (26), we obtain

$$\boldsymbol{B}_u = \begin{pmatrix} I_a(a_{\mathrm{ss}}) & 0 & 0 \\ 0 & 0 & 0 \\ 0 & 0 & k^2 I_\phi(a_{\mathrm{ss}}) \end{pmatrix}, \ \boldsymbol{b}^\top = \begin{pmatrix} 0 & 0 & kI_\phi(a_{\mathrm{ss}}) \end{pmatrix}, \ B_l = I_\phi(a_{\mathrm{ss}}). \tag{34}$$

In terms of the notation

$$\boldsymbol{g} = \begin{pmatrix} \mathfrak{g}_1 & \mathfrak{g}_2 & \mathfrak{g}_3 \end{pmatrix}, \ \boldsymbol{J}^{-1} = \begin{pmatrix} \mathfrak{i}_{11} & \mathfrak{i}_{12} & \mathfrak{i}_{13} \\ \mathfrak{i}_{21} & \mathfrak{i}_{22} & \mathfrak{i}_{23} \\ \mathfrak{i}_{31} & \mathfrak{i}_{32} & \mathfrak{i}_{33} \end{pmatrix}, \tag{35}$$

the corresponding asymptotic diffusion constant then equals

$$\mathrm{D}_\phi = (\mathfrak{g}_1\mathfrak{i}_{11} + \mathfrak{g}_2\mathfrak{i}_{21} + \mathfrak{g}_3\mathfrak{i}_{31})^2 I_a(a_{\mathrm{ss}}) + (1 - k(\mathfrak{g}_1\mathfrak{i}_{13} + \mathfrak{g}_2\mathfrak{i}_{23} + \mathfrak{g}_3\mathfrak{i}_{33}))^2 I_\phi(a_{\mathrm{ss}}). \tag{36}$$

The expression in Eq. (36) suggests that the terms that multiply $I_a(a_{\mathrm{ss}})$ and $I_\phi(a_{\mathrm{ss}})$ may both be eliminated by a suitable choice of adaptive feedback design and numerical value of k (unless the coefficient multiplying k vanishes, in which case we cannot modify the factor of $I_\phi(a_{\mathrm{ss}})$). In comparison, for standard oscillators, the coefficient of $I_a(a_{\mathrm{ss}})$ is associated with amplitude-to-frequency (A-F) noise conversion arising from dispersion and can be reduced or eliminated by running at small amplitudes or near special zero-dispersion points, which can be realized in both single-mode [10, 11] and coupled-mode operation [22]. As discussed in Sec. II E, near-resonant mode coupling affords an alternative means of realizing nonzero (but necessarily rational values of) k.

In the next subsection, we apply the result in Eq. (36) to classes of feedback designs that include those investigated numerically in Sec. III.

B. Model predictions

Many possibilities exist for the selection of adaptive control laws for the secondary loop. Here, we focus on classes of feedback designs that are simple yet offer the possibility of significantly reducing, or even eliminating (to leading asymptotic order) phase diffusion. These include the feedback designs introduced in the motivating results of Sec. III. In this section, we use Eq. (36) to provide the theoretical basis for these and other design choices. As in Sec. III, we limit the analysis to the case $f(a, T) = -T$ (but see Sec. II E) and select controllers that preserve the stable steady operating amplitude obtained in the absence of noise and the secondary loop, namely, $a = a_{\mathrm{ss}} := S \sin \Delta/2$. Some generalizations are discussed in Sec. IV C.

Feedback design (i) in Sec. III is a special case of a class of designs with $f_T = -G_T(T - T_{\mathrm{ss}})$, and $f_\theta = -G_\theta \theta$ (recall that $\theta_{\mathrm{ss}} = 0$), where the constants $G_T, G_\theta > 0$ ensure that T and θ converge exponentially fast to T_{ss} and 0, respectively. In the absence of noise, the steady condition given by $a = a_{\mathrm{ss}}$, $T = T_{\mathrm{ss}}$, and $\theta = 0$ is then invariant and locally exponentially attracting. In the limit of small noise, linearization yields a system of the form of Eq. (27)

with $\boldsymbol{g}$ and $\boldsymbol{J}$ obtained from

$$\mathfrak{g}_1 = \frac{3\gamma a_{\rm ss}^3 + 4a_{\rm ss}\cot\Delta - 2T_{\rm ss}}{4a_{\rm ss}^2},\ \mathfrak{g}_2 = \frac{1}{2a_{\rm ss}},\ \mathfrak{g}_3 = 0 \tag{37}$$

and

$$\mathfrak{i}_{11} = -1,\ \mathfrak{i}_{13} = \frac{T_{\rm ss}}{2G_\theta},\ \mathfrak{i}_{22} = -\frac{1}{G_T},\ \mathfrak{i}_{33} = -\frac{1}{G_\theta},\ \mathfrak{i}_{12} = \mathfrak{i}_{21} = \mathfrak{i}_{23} = \mathfrak{i}_{31} = \mathfrak{i}_{32} = 0. \tag{38}$$

The corresponding asymptotic diffusion constant equals

$$\begin{aligned}\mathrm{D}_\phi = {} & \left(\frac{3\gamma a_{\rm ss}^3 + 4a_{\rm ss}\cot\Delta - 2T_{\rm ss}}{4a_{\rm ss}^2}\right)^2 I_a(a_{\rm ss}) \\ & + \left(1 - \frac{kT_{\rm ss}(3\gamma a_{\rm ss}^3 + 4a_{\rm ss}\cot\Delta - 2T_{\rm ss})}{8a_{\rm ss}^2 G_\theta}\right)^2 I_\phi(a_{\rm ss}).\end{aligned} \tag{39}$$

Note that D_ϕ reduces to $I_\phi(a_{\rm ss})$ independently of the value of k precisely when the $I_a(a_{\rm ss})$ term is eliminated by setting

$$T_{\rm ss} = \frac{(3\gamma a_{\rm ss}^2 + 4\cot\Delta)a_{\rm ss}}{2}. \tag{40}$$

With this choice, no benefit results from a non-zero value of k. The latter is true also for the case that $T_{\rm ss} = 0$ as this corresponds asymptotically to the absence of the secondary feedback loop for which

$$\mathrm{D}_\phi = \left(\frac{3\gamma a_{\rm ss}^2 + 4\cot\Delta}{4a_{\rm ss}}\right)^2 I_a(a_{\rm ss}) + I_\phi(a_{\rm ss}). \tag{41}$$

With the numerical values in Sec. III, we obtain the minimum value $\mathrm{D}_\phi \approx 1.2\times 10^{-4}$ for (from Eq. (40)) $T_{\rm ss} = 81/16$, compared with the reference value $\mathrm{D}_\phi \approx 3.2\times 10^{-4}$ for $T_{\rm ss} = 0$. These predictions are in excellent agreement with the numerical results (cf. Figs. 3 and 5).

Per the closed-form expression for D_ϕ in Eq. (36), the simultaneous vanishing in Eq. (39) of the coefficient of $I_a(a_{\rm ss})$ and the coefficient of k in the factor multiplying $I_\phi(a_{\rm ss})$ is a consequence of the independence of f_T on a and θ, since then $\mathfrak{i}_{21} = \mathfrak{i}_{23} = 0$ and, already, $\mathfrak{g}_3 = 0$. Indeed, such simultaneous vanishing holds true as long as f_T is independent of θ, since then $\mathfrak{i}_{11}\mathfrak{i}_{23} = \mathfrak{i}_{21}\mathfrak{i}_{13}$. In contrast, taking $f_T = -G_T(T - T_{\rm ss}) + G_{\theta T}\theta$ and $f_\theta = -G_\theta\theta$ for $G_T, G_\theta > 0$ and $G_{\theta T} \neq 0$, then the coefficient of $I_a(a_{\rm ss})$ in Eq. (39) remains unchanged, while the coefficient of k in the factor multiplying $I_\phi(a_{\rm ss})$ in Eq. (39) changes to

$$\frac{T_{\rm ss}(3\gamma a_{\rm ss}^3 + 4a_{\rm ss}\cot\Delta - 2T_{\rm ss})}{8a_{\rm ss}^2 G_\theta} - \frac{G_{\theta T}}{2a_{\rm ss}G_T G_\theta}. \tag{42}$$

In this case, the assignment in Eq. (40) results in

$$\mathrm{D}_\phi = \left(1 + \frac{kG_{\theta T}}{2a_{\mathrm{ss}}G_T G_\theta}\right)^2 I_\phi(a_{\mathrm{ss}}), \tag{43}$$

which vanishes when $k = -2a_{\mathrm{ss}}G_T G_\theta / G_{\theta T}$, a marked improvement over the previous design.

Further inspection of Eq. (36) shows that the coefficient of $I_a(a_{\mathrm{ss}})$ may be eliminated for arbitrary T_{ss} by designing f_T and f_θ such that $\mathfrak{i}_{11} = \mathfrak{i}_{21} = 0$. By Cramer's rule, this follows if f_T and f_θ are both independent of θ, e.g., $f_T = G_{aT}(a - a_{\mathrm{ss}}) + G_{TT}(T - T_{\mathrm{ss}})$ and $f_\theta = G_{a\theta}(a - a_{\mathrm{ss}}) + G_{T\theta}(T - T_{\mathrm{ss}})$, where the gain coefficients are chosen such that the matrix

$$\boldsymbol{J} = \begin{pmatrix} -1 & 0 & -T_{\mathrm{ss}}/2 \\ G_{aT} & G_{TT} & 0 \\ G_{a\theta} & G_{T\theta} & 0 \end{pmatrix} \tag{44}$$

is Hurwitz. This case corresponds to feedback designs (ii) and (iii) in Sec. III. Here, in the absence of noise, the line $a = a_{\mathrm{ss}} := S \sin \Delta/2$, $T = T_{\mathrm{ss}}$, and $\theta = 0$ is again invariant and locally exponentially attracting. In the limit of small noise, the corresponding asymptotic diffusion constant equals

$$\mathrm{D}_\phi = \left(1 - k\frac{-2a_{\mathrm{ss}}G_{aT} + G_{TT}(-2T_{\mathrm{ss}} + 3\gamma a_{\mathrm{ss}}^3 + 4a_{\mathrm{ss}}\cot\Delta)}{4a_{\mathrm{ss}}^2(G_{a\theta}G_{TT} - G_{aT}G_{T\theta})}\right)^2 I_\phi(a_{\mathrm{ss}}), \tag{45}$$

which vanishes when

$$k = k_{\mathrm{opt}} := \left(\frac{-2a_{\mathrm{ss}}G_{aT} + G_{TT}(-2T_{\mathrm{ss}} + 3\gamma a_{\mathrm{ss}}^3 + 4a_{\mathrm{ss}}\cot\Delta)}{4a_{\mathrm{ss}}^2(G_{a\theta}G_{TT} - G_{aT}G_{T\theta})}\right)^{-1}, \tag{46}$$

provided that $-2a_{\mathrm{ss}}G_{aT} + G_{TT}(-2T_{\mathrm{ss}} + 3\gamma a_{\mathrm{ss}}^3 + 4a_{\mathrm{ss}}\cot\Delta) \neq 0$. With the numerical values in Sec. III, we obtain the value $\mathrm{D}_\phi \approx 1.2 \times 10^{-4}$ for $k = 0$ and $\mathrm{D}_\phi = 0$ for $k = k_{\mathrm{opt}} = 216/89$. These predictions are in excellent agreement with the numerical results (cf. Figs. 3 and 5). For these same parameter values, Fig. 6 shows a graphical representation of Eqs. (45) and (46).

C. Discussion of the Control Laws

As discussed below, the results in the previous section compare favorably to those obtained in the absence of secondary feedback, and illustrate how the introduction of secondary feedback can result in dramatic suppression of phase diffusion.

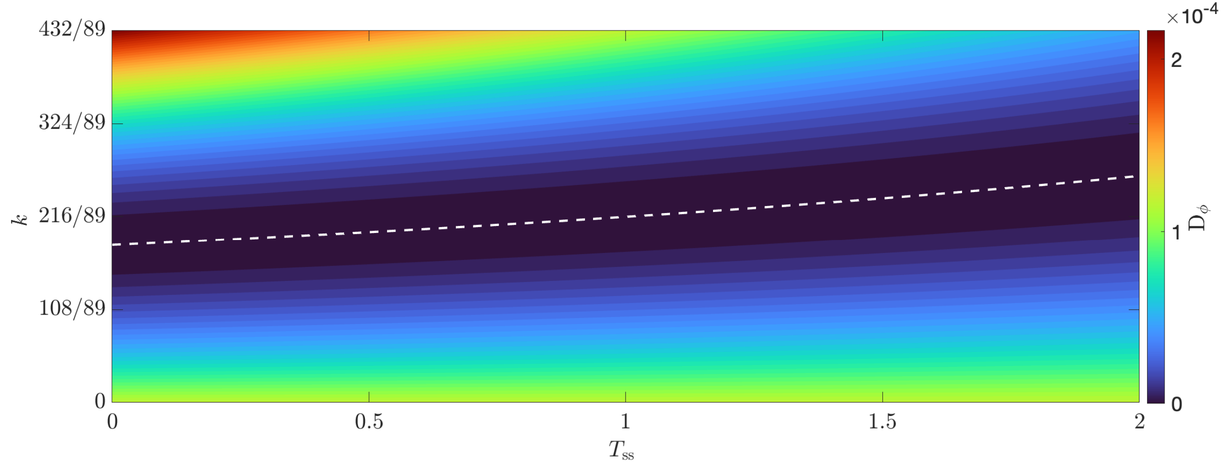

FIG. 6. Dependence of D_ϕ on T_{ss} and k from Eq. (45) for the set of model and gain parameters: $\gamma = 1, \Delta = \pi/2, G_{\theta T} = G_{\theta\theta} = 0, 2G_{aT} = -2G_{TT} = 2G_{a\theta} = G_{T\theta} = 2, a_{\mathrm{ss}} = 3/2$ and $\mathcal{I}_\xi = \mathcal{I}_\eta = 10^{-4}$. The white dashed curve depicts k_{opt} versus T_{ss} from Eq. (46).

It is straightforward to see that the asymptotic analysis in Sec. IV A applies also to the state-space dynamics

$$\begin{pmatrix} a' \\ \phi' \end{pmatrix} = \begin{pmatrix} f_a(a,0,\cdot) \\ f_\phi(a,0,\cdot) \end{pmatrix} + \sqrt{\boldsymbol{I}_{\boldsymbol{\chi}}}\boldsymbol{\chi}(s) \tag{47}$$

obtained from Eq. (25) by eliminating the secondary feedback loop. In the notation of Sec. IV A, we obtain

$$\boldsymbol{B}_u = \Big(I_a(a_{\mathrm{ss}})\Big)\,, \; \boldsymbol{b} = \Big(0\Big)\,, \; B_l = I_\phi(a_{\mathrm{ss}}),\; \boldsymbol{g} = \Big(\partial_a f_\phi(a_{\mathrm{ss}},0,\cdot)\Big)\,, \; \boldsymbol{J} = \Big(\partial_a f_a(a_{\mathrm{ss}},0,\cdot)\Big)\,, \tag{48}$$

from which we predict the asymptotic diffusion constant

$$\mathrm{D}_\phi = \left(\frac{\partial_a f_\phi(a_{\mathrm{ss}},0,\cdot)}{\partial_a f_a(a_{\mathrm{ss}},0,\cdot)}\right)^2 I_a(a_{\mathrm{ss}}) + I_\phi(a_{\mathrm{ss}}). \tag{49}$$

Here, $\Omega(a) := 1 + \varepsilon f_\phi(a,0,\cdot)$ is the frequency-amplitude dispersion relationship whose derivative $\Omega'(a)$ corresponds to the gain by which variations in amplitude convert to variations in frequency. From the expression for D_ϕ, we see that such conversion, when present, is responsible for a non-vanishing coefficient of $I_a(a_{\mathrm{ss}})$. For example, given the expression for f_ϕ in Eq. (10) and in the case that $\Delta = \pi/2$ and $\gamma \neq 0$, $\Omega'(a_{\mathrm{ss}}) := \partial_a f_\phi(a_{\mathrm{ss}},0,\cdot) = 3\gamma a_{\mathrm{ss}}/4$ is nonzero for all nonzero a_{ss} and the resonator nonlinearity degrades the oscillator's frequency stability as the oscillation amplitude increases; this is amplitude-frequency (A-F) noise conversion [31].

For a single-mode oscillator with a properly designed nonlinearity (i.e., a modified form of $f_\phi(a, 0, \cdot)$), the frequency-amplitude dispersion may be made non-monotone, such that $\Omega'(a_{\mathrm{ss}})$ vanishes at some locally unique a_{ss} known as a zero-dispersion (ZD) point [10, 11]. At such a point, D_ϕ then reduces to $I_\phi(a_{\mathrm{ss}})$ just as was obtained in the previous section with T_{ss} given by Eq. (40). The latter, however, applies across the entire viable range of values of a_{ss} and is neither limited to a unique value of a_{ss} nor constrained by the need for proper design of the oscillator nonlinearity.

It is clear from Eq. (36) that a lower bound for D_ϕ when $k = 0$ is $I_\phi(a_{\mathrm{ss}})$. In this case, one can select a_{ss} as large as feasible so as to approach from above the large amplitude limit $\mathrm{D}_\phi \sim 3\mathcal{I}_\eta/4$ (see Eq. (13)) that is set by the intrinsic frequency fluctuations of the resonator. It is only by taking advantage of nonzero values of k that the last two adaptive feedback designs in Sec. IV B are able to improve frequency stability further. They do so by operating in a phase-coupled condition for which $\theta = \psi + k\phi \approx 0$ and by steering a scaled version of the noise $\chi_2(s)$ that drives ϕ into the secondary feedback loop, allowing T and θ to respond accordingly.

V. CONCLUSIONS

In this work, we presented a method for suppressing noise-induced phase diffusion in a resonator with self-sustaining oscillations due to a primary feedback loop by using a secondary feedback loop with feedback-controlled amplitude and phase shift. As motivation for our feedback design and to verify our theoretical predictions, we simulated the fully nonlinear and stochastic slow amplitude and phase dynamics over large collections of sample noise histories. We found that the ensemble statistics of the numerical simulations of the fully nonlinear model agree remarkably well with the theoretical predictions, which are based on an asymptotic analysis of closed-form solutions of the noisy equations linearized about a stable nonlinear operating state.

The specific feedback designs considered in the previous sections were linear in the deviations of a, T, and θ from their steady-state values. In all cases, the amplitude factor $f(a, T)$ was chosen to equal $-T$. That neither is a limiting assumption on the applicability of the analysis was evidenced by the highly non-trivial slow amplitude and phase dynamics obtained from the equations modeling nearly phase-locked dynamics of coupled oscillator modes in the presence of an approximate internal resonance. Indeed, since the result in Eq. (36) was derived without any assumptions on $f(a,T)$ or linearity of f_T and f_θ, the corresponding expression for D_ϕ applies to both cases of internal resonance and may be used to explain experimental observations of coupled-mode resonators.

Importantly, we found that (i) complex coupling among the variables a, T, and θ, as found for the coupled-mode oscillators, is not necessary to improve frequency stability; and (ii) that the restriction to integer values of k may prevent optimal use of phase coupling. Instead, we showed that the proposed control architecture enables one to tailor the actuation from the secondary loop with a degree of flexibility and in parameter domains not achievable in physical single- or multiple-mode oscillators. In particular, we showed that we can design the secondary loop in ways that generate noise filtering characteristics that are impossible to realize in a standard oscillator configuration. For example, one design results in an oscillator with the equivalent of zero A-F conversion regardless of the operating amplitude, and another design utilizes phase coupling to theoretically reduce the phase diffusion to zero, realizing and surpassing the benefits of zero-dispersion and mode-coupling with potentially simpler engineering.

Our theoretical and numerically validated findings serve as motivation for the implementation of the described method in physical devices. We considered two paths to such realization, one in terms of two-mode operation with suitable physical coupling at the fast timescale, and one in terms of single-mode operation with regulation only on the slow timescale. In the latter case, we noted challenges with measuring the phase ϕ, or at least changes in ϕ over a slow timescale. While we proposed the possibility of self-referencing demodulation using a delay line, it remains an open question whether this would introduce stochastic effects that would outweigh the benefits of the secondary feedback. Other issues that need to be considered for the realization of the secondary loop using hardware or software include the effects of noise and uncertainties in the secondary feedback loop, which might arise, for example, from sampling and/or delay effects or noise in circuits. A study that points to the potential feasibility of the proposed approach is represented in [34], where small control pulses are applied at times based on a slowly varying amplitude of a MEMS device undergoing a complicated coupled-mode response. Given this, we view the results presented here as motivation to explore the implementation of slowly varying control to improve frequency stability.

Acknowledgments

OS is grateful for support from the ISF grant number 344/22 and the Pearlstone Center of Aeronautical Engineering Studies at BGU. SWS acknowledges support from the Defense Advanced Research Projects Agency (DARPA) H6 program under cooperative agreement HR0011-23-2-0004. This work is based upon research performed while HD was supported by and serving at the National Science Foundation. Any opinion, findings, and conclusions or recommendations expressed in this material are those of the authors and do not necessarily reflect the views of the National Science Foundation. We are grateful to Scott Strachan, Gaurav Bahl, Jintark Kim, Jie Yan, and Dave Czaplewski for helpful discussions.

Appendix A: Stochastic averaging

Given Eqs. (7) and (8), let

$$\zeta_1(\tau) = -\xi(s)\sin(\tau+\phi) + \frac{a\eta(s)}{2}\sin(2\tau+2\phi), \tag{A1}$$

$$\zeta_2(\tau) = -\frac{\xi(s)}{a}\cos(\tau+\phi) + \eta(s)\cos^2(\tau+\phi), \tag{A2}$$

where $s = \varepsilon\tau$. The method of stochastic averaging implies that

$$I_a(a)\left\langle \chi_1(s)\chi_1(s+\sigma)\right\rangle = \delta(\sigma)\int_{-\infty}^{\infty}\left\langle \zeta_1(\tau)\zeta_1(\tau+\tau')\right\rangle\,\mathrm{d}\tau', \tag{A3}$$

$$\sqrt{I_a(a)I_\phi(a)}\left\langle \chi_1(s)\chi_2(s+\sigma)\right\rangle = \delta(\sigma)\int_{-\infty}^{\infty}\left\langle \zeta_1(\tau)\zeta_2(\tau+\tau')\right\rangle\,\mathrm{d}\tau', \tag{A4}$$

$$I_\phi(a)\left\langle \chi_2(s)\chi_2(s+\sigma)\right\rangle = \delta(\sigma)\int_{-\infty}^{\infty}\left\langle \zeta_2(\tau)\zeta_2(\tau+\tau')\right\rangle\,\mathrm{d}\tau'. \tag{A5}$$

To dominant order in the analysis, oscillatory contributions that average to 0 on the fast timescale may be neglected in the integrands. It follows that

$$\begin{aligned}\left\langle \zeta_1(\tau)\zeta_1(\tau+\tau')\right\rangle &= \frac{\cos\tau'}{2}\left\langle \xi(\tau)\xi(\tau+\tau')\right\rangle + \frac{a^2\cos 2\tau'}{8}\left\langle \eta(\tau)\eta(\tau+\tau')\right\rangle \\ &= \left(I_\xi\cos\tau' + \frac{I_\eta a^2}{4}\cos 2\tau'\right)\delta(\tau'),\end{aligned} \tag{A6}$$

$$\begin{aligned}\left\langle \zeta_1(\tau)\zeta_2(\tau+\tau')\right\rangle &= -\frac{\sin\tau'}{2a}\left\langle \xi(\tau)\xi(\tau+\tau')\right\rangle - \frac{a\sin 2\tau'}{8}\left\langle \eta(\tau)\eta(\tau+\tau')\right\rangle \\ &= -\left(\frac{I_\xi}{a}\sin\tau' + \frac{I_\eta a}{4}\sin 2\tau'\right)\delta(\tau'),\end{aligned} \tag{A7}$$

and

$$\begin{aligned}\langle\zeta_2(\tau)\zeta_2(\tau+\tau')\rangle &= \frac{\cos\tau'}{2a^2}\left\langle\xi(\tau)\xi(\tau+\tau')\right\rangle + \left(\frac{1}{4}+\frac{\cos 2\tau'}{8}\right)\left\langle\eta(\tau)\eta(\tau+\tau')\right\rangle \\ &= \left(\frac{I_\xi}{a^2}\cos\tau' + I_\eta\left(\frac{1}{2}+\frac{\cos 2\tau'}{4}\right)\right)\delta(\tau'),\end{aligned} \tag{A8}$$

from which Eq. (13) and the correlations of χ_1 and χ_2 follow. The diffusion approximation relied upon to replace Eqs. (7) and (8) with Eqs. (11) and (12) also produces deterministic contributions to order $\mathcal{O}(\varepsilon^0)$. To compute these, let

$$\zeta_3(\tau) = \frac{\eta(s)}{2}\sin(2\tau+2\phi), \tag{A9}$$

$$\zeta_4(\tau) = -\xi(s)\cos(\tau+\phi) + a\eta(s)\cos(2\tau+2\phi), \tag{A10}$$

$$\zeta_5(\tau) = \frac{\xi(s)}{a^2}\cos(\tau+\phi), \tag{A11}$$

$$\zeta_6(\tau) = \frac{\xi(s)}{a}\sin(\tau+\phi) - \eta(s)\sin(2\tau+2\phi). \tag{A12}$$

Then, by again neglecting oscillatory terms that average to 0 on the fast timescale, this deterministic contribution to Eq. (11) is given by

$$\int_{-\infty}^{0}\left\langle\zeta_3(\tau)\zeta_1(\tau+\tau') + \zeta_4(\tau)\zeta_2(\tau+\tau')\right\rangle\,\mathrm{d}\tau' = \frac{I_\xi}{2a} + \frac{3aI_\eta}{8} \tag{A13}$$

while that to Eq. (12) is given by

$$\int_{-\infty}^{0}\left\langle\zeta_5(\tau)\zeta_1(\tau+\tau') + \zeta_6(\tau)\zeta_2(\tau+\tau')\right\rangle\,\mathrm{d}\tau' = 0. \tag{A14}$$

In the main analysis, we neglect the contribution from (A13) by focusing on the limiting case of small noise, for which $I_\eta \ll 1$ and $I_\xi \ll a^2$.

Data Availability Statement

A Matlab script sufficient to generate the numerical results reported here may be freely downloaded from [35]. Note that small deviations from the numerical results shown in Figs. 3-5 are expected, since the analysis relies on ensemble simulations of stochastic processes.

Author Contributions

HD: conceptualization, formal analysis, methodology, investigation, writing - original draft, review and editing. SS: methodology, writing – original draft, review and editing. OS: formal analysis, software, methodology, investigation, writing - review and editing.

---

[1] J. R. Vig, Quartz crystal resonators and oscillators for frequency control and timing applications. a tutorial, Nasa Sti/recon Technical Report N **95**, 19519 (1994).

[2] E. Rubiola, *Phase noise and frequency stability in oscillators* (Cambridge University Press, 2009).

[3] W. J. Riley and D. A. Howe, *Handbook of frequency stability analysis* (US Department of Commerce, National Institute of Standards and Technology . . . , 2008).

[4] M. Dykman and M. Krivoglaz, Soviet physics reviews, Harwood Academic, New York , 265 (1984).

[5] E. A. Vittoz and Y. P. Tsividis, Frequency-dynamic range-power, in *Trade-Offs in Analog Circuit Design: The Designer's Companion* (Springer, 2002) pp. 283–313.

[6] D. Greywall, B. Yurke, P. Busch, A. Pargellis, and R. Willett, Evading amplifier noise in nonlinear oscillators, Physical review letters **72**, 2992 (1994).

[7] B. Yurke, D. Greywall, A. Pargellis, and P. Busch, Theory of amplifier-noise evasion in an oscillator employing a nonlinear resonator, Physical Review A **51**, 4211 (1995).

[8] M. Dykman, R. Mannella, P. V. McClintock, S. M. Soskin, and N. Stocks, Noise-induced narrowing of peaks in the power spectra of underdamped nonlinear oscillators, Physical Review A **42**, 7041 (1990).

[9] J. Moehlis, Improving the precision of noisy oscillators, Physica D: Nonlinear Phenomena **272**, 8 (2014).

[10] L. Huang, S. Soskin, I. Khovanov, R. Mannella, K. Ninios, and H. B. Chan, Frequency stabilization and noise-induced spectral narrowing in resonators with zero dispersion, Nature communications **10**, 1 (2019).

[11] N. J. Miller, S. W. Shaw, and M. Dykman, Suppressing frequency fluctuations of self-sustained vibrations in underdamped nonlinear resonators, Physical Review Applied **15**, 014024 (2021).

[12] L. G. Villanueva, R. B. Karabalin, M. H. Matheny, E. Kenig, M. C. Cross, and M. L. Roukes, A nanoscale parametric feedback oscillator, Nano letters **11**, 5054 (2011).

[13] C. Cassella, S. Strachan, S. W. Shaw, and G. Piazza, Phase noise suppression through parametric filtering, Applied Physics Letters **110**, 063503 (2017).

[14] E. Kenig, M. Cross, L. Villanueva, R. Karabalin, M. Matheny, R. Lifshitz, and M. Roukes, Optimal operating points of oscillators using nonlinear resonators, Physical Review E **86**, 056207 (2012).

[15] E. Kenig, M. Cross, R. Lifshitz, R. Karabalin, L. Villanueva, M. Matheny, and M. Roukes, Passive phase noise cancellation scheme, Physical review letters **108**, 264102 (2012).

[16] L. Villanueva, E. Kenig, R. Karabalin, M. Matheny, R. Lifshitz, M. Cross, and M. Roukes, Surpassing fundamental limits of oscillators using nonlinear resonators, Physical review letters **110**, 177208 (2013).

[17] E. Kenig, M. Cross, J. Moehlis, and K. Wiesenfeld, Phase noise of oscillators with unsaturated amplifiers, Physical Review E **88**, 062922 (2013).

[18] D. Antonio, D. H. Zanette, and D. López, Frequency stabilization in nonlinear micromechanical oscillators, Nature communications **3**, 1 (2012).

[19] J. Yu, K. Asadi, H. Brahmi, H. Cho, S. Nezmi, and S. Lee, Frequency stabilization in a mems oscillator with 1: 2 internal resonance, in *2019 IEEE International Symposium on Inertial Sensors and Systems (INERTIAL)* (IEEE, 2019) pp. 1–4.

[20] J. Yu, H.-K. Kwon, G. D. Vukasin, T. W. Kenny, and H. Cho, Frequency stabilization in an encapsulated high-q micromechanical resonator via internal resonance, in *2020 IEEE 33rd International Conference on Micro Electro Mechanical Systems (MEMS)* (IEEE, 2020) pp. 1191–1194.

[21] J. Yu and H. Cho, Exploiting and tailoring 1: 2 internal resonance in a stepped beam micromechanical resonator for frequency stabilization, Sensors and Actuators A: Physical **362**, 114619 (2023).

[22] O. Shoshani, S. Strachan, D. Czaplewski, D. Lopez, and S. W. Shaw, Extraordinary frequency stabilization by resonant nonlinear mode coupling, Physical Review Applied **22**, 054055 (2024).

[23] O. Shoshani and S. W. Shaw, Resonant modal interactions in micro/nano-mechanical structures, Nonlinear Dynamics **104**, 1801 (2021).

[24] A. Donmez, H. Herath, and H. Cho, Theoretical insights into 1:2 and 1:3 internal resonance for frequency stabilization in nonlinear micromechanical resonators (2024), arXiv:2410.03109 [physics.app-ph].

[25] R. M. Mestrom, R. H. Fey, and H. Nijmeijer, Phase feedback for nonlinear mem resonators in oscillator circuits, IEEE/ASME Transactions on Mechatronics **14**, 423 (2009).

[26] H. K. Lee, R. Melamud, S. Chandorkar, J. Salvia, S. Yoneoka, and T. W. Kenny, Stable operation of mems oscillators far above the critical vibration amplitude in the nonlinear regime, Journal of microelectromechanical systems **20**, 1228 (2011).

[27] R. L. Stratonovich, *Topics in the theory of random noise*, Vol. 1 (Gordon and Breach, 1963).

[28] A. Keşkekler, O. Shoshani, M. Lee, H. S. van der Zant, P. G. Steeneken, and F. Alijani, Tuning nonlinear damping in graphene nanoresonators by parametric–direct internal resonance, Nature communications **12**, 1099 (2021).

[29] M. Hasan, C. Nicholls, K. Pitre, B. Spokoinyi, and T. Hall, Delay drift compensation of an optoelectronic oscillator over a large temperature range through continuous tuning, Communications Engineering **3** (2024).

[30] S. Johnson, S. Mishra, A. Pathak, and S. De, Frequency drift corrected ultra-stable laser through phase-coherent fiber producing a quantum channel, Communications Physics **8** (2025).

[31] A. Demir, A. Mehrotra, and J. Roychowdhury, Phase noise in oscillators: A unifying theory and numerical methods for characterisation, in *Proceedings of the 35th annual Design Automation Conference* (1998) pp. 26–31.

[32] M. Cross, Improving the frequency precision of oscillators by synchronization, Physical Review E—Statistical, Nonlinear, and Soft Matter Physics **85**, 046214 (2012).

[33] D. J. Higham, An algorithmic introduction to numerical simulation of stochastic differential equations, SIAM review **43**, 525 (2001).

[34] A. M. Eriksson, O. Shoshani, D. López, S. W. Shaw, and D. A. Czaplewski, Controllable branching of robust response patterns in nonlinear mechanical resonators, Nature communications **14**, 161 (2023).

[35] H. Dankowicz, O. Shoshani, and S. W. Shaw, `https://github.com/hdankowicz-umd/noise-suppression2025-scripts`, accessed: 2026-04-23.